Control Engineering Practice 21 (2013) 1776–1787

Contents lists available at ScienceDirect

Control Engineering Practice

journal homepage: www.elsevier.com/locate/conengprac

Flood control of the Demer by using Model Predictive Control

Maarten Breckpot [a,*], Oscar Mauricio Agudelo [a], Pieter Meert [b], Patrick Willems [b], Bart De Moor [a]

[a] KU Leuven Department of Electrical Engineering (ESAT-SCD)/iMinds Future Health Department, Kasteelpark Arenberg 10, B-3001 Leuven, Belgium
[b] KU Leuven Department of Civil Engineering, Kasteelpark Arenberg 40, B-3001 Leuven, Belgium

ARTICLE INFO

Article history:
Received 28 February 2013
Accepted 16 August 2013
Available online 3 October 2013

Keywords:
Model Predictive Control
Flood control
Kalman filter
Open channel flow

ABSTRACT

It is shown how Model Predictive Control can be used for flood control of river systems modelled with real data. A linear model for the Demer, a river in Belgium, is derived, which is used inside the optimisation problem solved by the controller. This optimisation problem is formulated such that the controller can be used for set-point and flood control. A Kalman filter is used as a state estimator. Closed loop simulations performed with a full hydrodynamic model of the Demer in combination with historical rainfall data show that the proposed control scheme outperforms the current control strategy.

© 2013 Elsevier Ltd. All rights reserved.

1. Introduction

River floods are worldwide a serious problem. One example of a river in Belgium with a long history of severe floods is the Demer. In order to reduce these floods, the local government has installed water reservoirs to store the excess of water during periods of heavy rainfall. Also hydraulic structures were built to control the discharges in the river and the water going to and coming from these reservoirs. Although these adaptations significantly reduced the risk of flooding along the Demer, extreme rainfalls in 1998 and 2002 still resulted in severe floods. Simulations performed by the government have shown that these floods could have been reduced or even avoided if a more advanced control strategy had been used. Previous works exist where Model Predictive Control (MPC) is successfully used for flood control and set-point control of the Demer based on a simple model. The goal of this research is to further improve these MPC schemes by working with an approximate model of a full hydrodynamic model of the Demer and test the controller on this white box model.

MPC (Mayne, Rawlings, Rao, & Scokaert, 2000; Rossiter, 2003) originates from the chemical process industry but it has shown great value in many different applications going from food processing to automotive and aerospace applications (Qin & Badgwell, 2003). Because MPC formulates the control problem as an optimisation problem, it can be used to control rivers during different operating conditions. By minimising the deviations of water levels from their targets, MPC will focus on set-point control during periods of no or little rainfall. By incorporating the flood levels as constraints on the water levels in the optimisation problem, the same MPC will focus on flood control during periods of heavy rainfall. However only a high control performance can be achieved if an accurate model is used in the optimisation problem.

The dynamics of a reach of a river can be modelled with the full hydrodynamic equations of de Saint-Venant, or the so-called Saint-Venant equations (Chow, Maidment, & Mays, 1988). Based on these equations together with the dynamics of hydraulic structures, junctions and reservoirs, a mathematical model can be derived for a river system. Because of the complexity of these models, MPC cannot work directly with these equations but use approximate models. Models derived by means of identification techniques or simple integrator delay models provide a good approximation and have been used in combination with MPC in many studies for set-point control (Puig et al., 2009; van Overloop, 2006; van Overloop, Clemmens, Strand, Wagemaker, & Bautista, 2010; Wahlin & Clemmens, 2006). However these models are not accurate enough for the purpose of flood control because they model the water levels at only one location. Therefore it is hard to guarantee that the water level profile along the entire reach is below the flood level. In previous works done by our research group a conceptual model was used to model the Demer (Barjas Blanco et al., 2010; Breckpot, Barjas Blanco, & De Moor, 2010; Barjas Blanco, 2010). However this model approximates the dynamics of every reach at only a very limited number of points. Because the flood levels are very irregular, it is never certain that

* Corresponding author. Tel.: +32 16328652; fax: +32 16321970.
E-mail addresses: maarten.breckpot@esat.kuleuven.be, maarten.breckpot@hotmail.com (M. Breckpot), mauricio.agudelo@esat.kuleuven.be (O.M. Agudelo), pieter.meert@bwk.kuleuven.be (P. Meert), patrick.willems@bwk.kuleuven.be (P. Willems), bart.demoor@esat.kuleuven.be (B. De Moor).

0967-0661/$ - see front matter © 2013 Elsevier Ltd. All rights reserved.
http://dx.doi.org/10.1016/j.conengprac.2013.08.008

no floods are present along the entire river if the limited number of water levels are below their flood levels. Therefore a model based on the linear approximation of the Saint-Venant equations along the entire river is used in this study. This model has already been used by the authors in combination with MPC in Breckpot, Agudelo, and De Moor (2013). However that study only focused on a small artificial academic test example, while in this paper the controller is applied to a white box model of a real river whose parameters are derived from real field data. MPC is used in combination with a Kalman filter (Kalman, 1960) which is used to estimate the entire state of the system at every time instant based on a limited number of measured water levels. Also a comparison is made with the performance of the current control strategy for the historical rainfall data of the Demer of 2002.

Contribution: In this work it is shown that MPC in combination with a Kalman filter can successfully be used for set-point control and flood control of river systems. The authors are not aware of any other publication where these techniques are successfully applied to a full hydrodynamical model whose parameters are derived from real river data to optimally use the buffer capacity of reservoirs for flood control. The main contributions lie in

- the derivation of the linear model used by the controller inside the optimisation problem,
- the formulation of the optimisation problem,
- the formulation of a fast nonlinear prediction step to estimate limits on the gate discharges and a simple procedure to update the linear models used inside the optimisation problem,
- the adaptation of the classical Kalman filter for getting accurate state estimates,
- and in showing that the controller outperforms the current control scheme by testing the controller on a real river case with historical rainfall data.

As it was already mentioned, there exist previous works where MPC is applied to a conceptual model (Barjas Blanco, 2010; Barjas Blanco et al., 2010; Breckpot et al., 2010). There are four major distinctions with these works:

- *Process model*: The previous works use a conceptual model with a limited number of nodes for simulating the Demer. In this paper a fully hydrodynamic model of the Demer is used for testing the control performance of the developed predictive controller resulting in more realistic simulations.
- *Control strategy*: Regarding the predictive controller, the main difference lies in the choice of the control variables used inside the optimisation problem. In the previous works the authors worked with the gate positions as optimisation variables resulting in the requirement to use nonlinear model based predictive control schemes in order to achieve a good control performance. At every time step a new sequence of time-varying linear state space models need to be derived over the prediction window based on the sequence of optimal control actions calculated at the previous time step. Because of the limited accuracy of the linear approximation of the gate equations, a trust region is used inside the optimisation problem in order to limit the difference between the new optimal sequence of control actions and the previous one. Furthermore a line search is used as post-processing step to increase the effectiveness of the computed control actions. As we will show these operations are not needed by working with the gate discharges as optimisation variables. Eliminating the gate equations out of the optimisation problem has as effect that the dynamics of the river systems can be accurately approximated with a linear state space model that needs to be derived only once: a linear predictive control scheme can be used. Another difference lies in how the upper limits on the water levels are imposed. The previous works impose these inequality constraints as hard constraints, which can lead to infeasibilities during periods of excessive rainfall. Therefore a constraint relaxation strategy is implemented that iteratively drops inequality constraints until the optimisation problem becomes feasible. This approach can result in solving multiple optimisation problems. This situation is avoided in this paper by working with slack variables and imposing the inequality constraints as soft constraints. Following this approach results in an optimisation problem that is always feasible.
- *State estimator*: Because the previous works use the gate positions as control variables, Moving Horizon Estimation (MHE) was used as estimation technique. This technique results in solving an optimisation problem at every time step taking the measurements of the last sampling times into account as well. In this study, by working with the gate discharges as control variables, MHE is not longer required to obtain accurate estimates of the unknown states. It is shown that a Kalman filter is accurate enough requiring only a limited number of operations at every time step.

Paper outline: Section 2 introduces the part of the Demer that is modelled and controlled in this work together with the control objectives. Section 3 explains how river systems can be modelled and also describes the model developed for the upstream part of the Demer. Section 4 briefly discusses the current control strategy while Section 5 explains in detail how MPC can be used for flood control. Section 6 presents the Kalman filter used for estimating the states. Section 7 compares the performance of the current control strategy with MPC for historical rainfall data of the Demer. This paper ends with Section 8 with some conclusions and future work.

Notation: Matrices are denoted with bold capital letters, e.g. $\boldsymbol{X}$, while bold lowercase letters are used for vectors, e.g. $\boldsymbol{x}$. Scalars or entries of vectors are not bold. The ith component of $\boldsymbol{x}$ is denoted by x_i. $\|\boldsymbol{x}\|_{\boldsymbol{W}}^2$ denotes $\boldsymbol{x}^T\boldsymbol{W}\boldsymbol{x}$. Superscript (i) indicates the channel, gate or reservoir the variable or parameter belongs to. $\mathbf{1}_n$ represents a vector of ones of dimension n. The following symbols and abbreviations are used throughout the paper:

g	the gravitational acceleration constant (m s^{-2})
t	the time variable (s)
z	the spatial variable (m)
$\boldsymbol{A}, \boldsymbol{B}, \boldsymbol{D}$	the state space matrices of the discrete time model: $\boldsymbol{x}(k+1)=\boldsymbol{A}\boldsymbol{x}(k)+\boldsymbol{B}\boldsymbol{u}(k)+\boldsymbol{D}\boldsymbol{d}(k)$
$\boldsymbol{x}$	the state vector
$\boldsymbol{u}$	the vector of control actions
$\boldsymbol{d}$	the vector of disturbances
A	the cross-sectional flow area (m^2)
B	the bottom width of a trapezoidal channel (m)
h	the water level (m)
L	the channel length (m)
n_{mann}	the Manning coefficient (s m$^{-1/3}$)
n_{eqmann}	the equivalent Manning coefficient (s m$^{-1/3}$)
P	the wetted perimeter of a cross section (m)
Q	the water discharge (m^3 s^{-1})
R	the hydraulic radius of a cross section (m)
S_0	the bed slope (–)
S_1, S_2	the side slopes of a trapezoidal channel (–)
S_f	the friction slope (–)
MPC	Model Predictive Control
PDE	Partial Differential Equation
QP	Quadratic Programming problem

TAW	reference height for altimetry in Belgium
VMM	Flemish Environment Agency

2. The study area and control objectives

Fig. 1 gives a schematic overview of a large part of the Demer together with its tributaries, water reservoirs and hydraulic structures. Because this is the first time the proposed control scheme is tested on white box modelled based on real river data, this paper focusses only on the upstream part of the Demer in the red rectangle area of Fig. 1 with the assumption that the reservoir Schulensmeer is directly connected to the Demer through gate D (similarly as the models used in Barjas Blanco, 2010; Barjas Blanco, Willems, Po-Kuan Chiang, Cauwenberghs, & De Moor, 2009; Breckpot et al., 2010). Fig. 2 shows the part of the Demer that will be modelled and controlled in this work. Section 3 explains how a mathematical model is constructed for this part of the Demer. This upstream part contains the Demer and its tributary Mangelbeek, gates A, K7 and D and the reservoir Schulensmeer. Gates A and D can be used to control the water flowing between the Demer and the reservoir. Gate K7 can be used to control the water levels in the Demer and the Mangelbeek. Historical data will be used to model the incoming discharges upstream of the Demer and the Mangelbeek, resp. Q_{Dem} and Q_{Man}. The Demer itself consists of four reaches (Dem_1 until Dem_4) while the Mangelbeek contains one reach (Man_5). During normal operation the controller should focus on set-point control by keeping h_{up} as close as possible to 21.5 m TAW (where TAW is the reference height for altimetry in Belgium) without increasing the water level h_s of the reservoir. During a period of heavy rainfall, the buffer capacity of the reservoir cannot be used as long as any of the water levels stay below their given safety limits. Once the model predicts a future violation of these safety limits, the buffer capacity of the reservoir can be used until its own safety limit is reached. In this situation the water levels of the reaches are allowed to further increase until the moment that they violate their flood levels. At that moment the last remaining buffer capacity can be used. After a period of heavy rainfall the water level of the reservoir should be decreased as fast as possible to its original height of 20.4 m TAW in order to have sufficient buffer capacity for possible future rainfall. After recovering the buffer capacity the controller should focus again on set-point control. Every hydraulic structure has an upper and lower limit on the gate position together with a rate of change constraint.

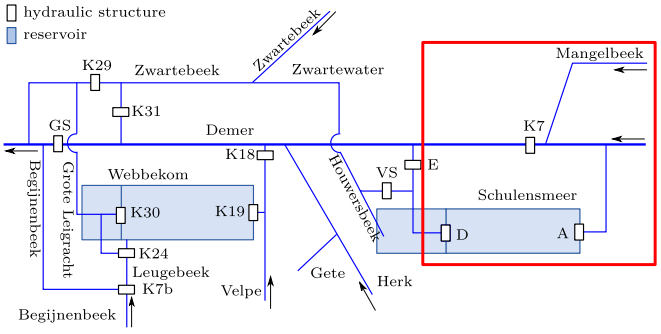

Fig. 1. Schematic overview of the Demer.

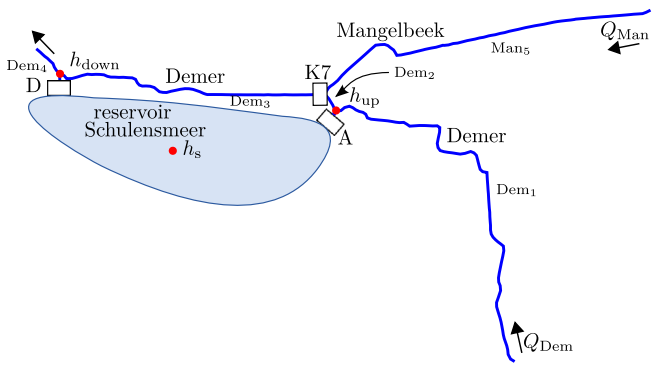

Fig. 2. Upstream part of the Demer that is modelled and controlled in this study.

3. Modelling

3.1. Single reach

The standard approach in the literature to model the dynamics of a single reach without lateral inflow is by using the full hydrodynamic equations of de Saint-Venant (Chaudry, 2008; Cunge, Holly, & Verwey, 1980; Litrico & Fromion, 2009; Sturm, 2001):

$$\frac{\partial A(z,t)}{\partial h(z,t)}\frac{\partial h(z,t)}{\partial t}+\frac{\partial Q(z,t)}{\partial z}=0, \tag{1}$$

$$\frac{\partial Q(z,t)}{\partial t}+\frac{\partial}{\partial z}\frac{Q(z,t)^2}{A(z,t)}+gA(z,t)\left(\frac{\partial h(z,t)}{\partial z}+S_f(z,t)-S_0\right)=0, \tag{2}$$

where t is the time variable (s), z is the space variable (m), $Q(z,t)$ the water discharge ($\text{m}^3\ \text{s}^{-1}$), $h(z,t)$ the water depth [m], $A(z,t)$ the cross-sectional flow area (m^2), g the gravity acceleration ($\text{m}\ \text{s}^{-2}$), S_0 the river bed slope and $S_f(z,t)$ the friction slope. Eq. (1) describes the conservation of mass and Eq. (2) the conservation of momentum. The friction slope $S_f(z,t)$ is modelled in this study with the resistance law of Manning (Chow, 1959):

$$S_f(z,t)=\frac{n_{\text{mann}}^2 Q(z,t)|Q(z,t)|}{A(z,t)^2 R(z,t)^{1/3}} \tag{3}$$

where n_{mann} is the Manning coefficient ($\text{sm}^{-1/3}$), $R(z,t)=A(z,t)/P(z,t)$ the hydraulic radius (m) and $P(z,t)$ is the wetted perimeter of the cross section (m). The reaches of the Demer have an irregular bed slope and an irregular cross section as shown in Fig. 3, where L is the length of the channel (m). As will be explained in Section 5.1, these cross sections will be approximated using an optimisation procedure with a trapezoidal shape with side slopes S_1 and S_2 and bottom width B (m) when we derive the approximate model used by the controller. The parameters of a trapezoidal channel can be seen in Fig. 4. However, the irregular

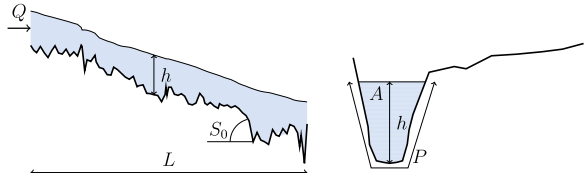

Fig. 3. The bed level of the Mangelbeek (left) and an example of a cross sectional profile (right).

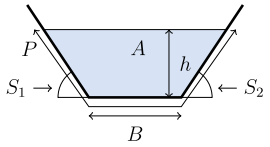

Fig. 4. Parameters of a trapezoidal channel.

cross sections will be used at the moment of performing the closed-loop simulations.

Every irregular cross section consists of a piecewise linear profile where one specific Manning coefficient is defined for every linear segment. The coefficients for the segments in the lower part of the river bed are typically smaller than the coefficients for the segments in the higher part or close to the flood levels because of their difference in roughness. One needs to calculate an equivalent Manning coefficient based on the current water level for every section every time Eq. (3) is evaluated. By assuming that the mean flow velocity over every subdivision i is equal to the mean flow velocity over the entire section (Horton, 1933), the equivalent Manning coefficient can be calculated with

$$n_{\text{mann}} = \left(\frac{\sum_{i=1}^{m} P_i n_{\text{mann},i}^{3/2}}{\sum_{i=1}^{m} P_i} \right)^{2/3} \tag{4}$$

where $n_{\text{mann},i}$ is the Manning coefficient for the ith linear segment with a wetted perimeter P_i and m the number of segments (partially) under water.

The Partial Differential Equations (PDEs) (1) and (2) will be used to model the dynamics of the five reaches Dem_1, Dem_2, Dem_3, Dem_4 and Man_5. Together with these PDEs, upstream and downstream boundary conditions are needed for each channel. The most simple boundary condition is a given upstream or downstream discharge. Applied to Fig. 2 this corresponds with the disturbance signals Q_{Dem} and Q_{Man} for resp. the most upstream reach of the Demer (Dem_1) and the Mangelbeek (Man_5). Other possibilities are gates and junctions.

3.2. Hydraulic structures

The hydraulic structures used in this paper are gated weirs as visualised in Fig. 5. h_1 and h_2 are the up- and downstream water levels of the gate respectively and c is the gate position. The hydraulic structure equations used in this work are based on the equations used in an existing full hydrodynamic model implemented in the InfoWorks-RS software (Innovyze, 2011) built for the Flemish Environment Agency (Willems et al., 2008). The algebraic equation of the gate presented in Fig. 5 is as follows:

$$Q^{(gate)}(t) = \tilde{f}(c(t), h_1(t), h_2(t)), \tag{5}$$

where $\tilde{f}$ is a nonlinear scalar function (Innovyze, 2011) and $Q^{(gate)}$ is the discharge over the gate. The specific form of this equation depends on the flow condition of the gate. If the gate position c is too small in comparison with h_1 and h_2, the gate position itself has no influence on the discharge over the gate, and the gate is said to be in the throat control mode. If the gate position has an influence on the discharge over the gate, then the gate is said to be in gate control mode. This gate equation can be used to model the connection between Dem_2 and Dem_3 through gate K7:

$$Q^{(2)}(L^{(2)}, t) = Q^{(3)}(0, t), \tag{6}$$

$$Q^{(3)}(0, t) = \tilde{f}(c^{(\text{K7})}(t), h^{(2)}(L^{(2)}t), h^{(3)}(0, t)). \tag{7}$$

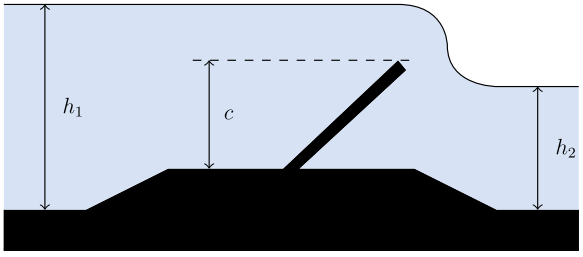

Fig. 5. Gated weir.

This simply means that the discharge leaving Dem_2 is equal to the discharge entering Dem_3 and they are equal to the gate discharge. A similar reasoning holds for gates A and D.

3.3. Junctions

Junctions are places where three or more reaches coincide or where a reach or reservoir is connected via an hydraulic structure to two other reaches. Examples for the Demer are

- gate A connecting the reservoir with Dem_1 and Dem_2,
- gate D connecting the reservoir with Dem_3 and Dem_4
- and gate K7 connecting Dem_3 with Dem_2 and Man_5.

The water levels of the reaches at these junctions should be equal and the sum of the discharges entering the junction should be equal to the sum of the discharges leaving the junction. Applying this to the first junction results in the following equations:

$$h^{(1)}(L^{(1)}, t) = h^{(2)}(0, t), \tag{8}$$

$$Q^{(1)}(L^{(1)}, t) = Q^{(2)}(0, t) + Q^{(\text{A})}(t). \tag{9}$$

Similar equations can be derived for the other two junctions.

3.4. Reservoirs

The reservoir Schulensmeer is modelled as one large tank. The change in volume is related to the water entering and leaving through gates A and D:

$$dV_s/dt = Q^{(\text{A})}(t) - Q^{(\text{D})}(t) \tag{10}$$

with V_s the volume of the reservoir (m^3). This volume depends in a nonlinear way on the water level h_s of the reservoir. The nonlinear relation used in this work is based on the conceptual model developed for this reservoir, based on detailed topographical data, by Willems et al. (2008) and Chiang and Willems (2010). It has the following form:

if $h_s < 20.38$

$$V_s = (h_s - 20.38)/0.000771 \tag{11}$$

else

$$V_s = ((h_s - 20.38)/0.000771)^{(1/0.838549)}. \tag{12}$$

More information on how these equations are derived can be found in Chiang and Willems (2010).

3.5. Downstream boundary condition

The downstream boundary condition for Dem_4 will be modelled with the following rating curve (Willems et al., 2008):

$$h^{(4)}(L^{(4)}, t) = 0.9722 \cdot Q(L^{(4)}, t)^2. \tag{13}$$

3.6. Discretisation and numerical implementation

Since there is no analytical solution for the Saint-Venant equations, the infinite dimensional variables are approximated on a finite grid (Strelkoff & Falvey, 1993). The partial derivatives are approximated with finite differences while the θ-method, e.g. $f(t_k + \theta\Delta t) = \theta f(t_k + \Delta t) + (1-\theta) f(t_k)$ with $\theta \in [0, 1]$ and Δt the

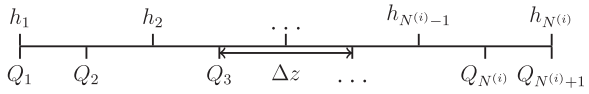

Fig. 6. Staggered grid structure used to discretise the Saint-Venant equations.

integration step, is used for the time integration. A staggered grid (see Fig. 6) with $N^{(i)}$ water levels and $N^{(i)}+1$ discharges for a given channel i is used for the spatial discretisation. The derivatives in Eq. (1) are approximated by (note $Q^{(i)}(z_j,t_k)=Q^{(i)}_{j,k}$ and $Q^{(i)}_{j,k+\theta}=\theta Q^{(i)}_{j,k+1}+(1-\theta)Q^{(i)}_{j,k}$)

$$\frac{\partial h^{(i)}_{j,k}}{\partial t}\simeq\frac{h^{(i)}_{j,k+1}-h^{(i)}_{j,k}}{\Delta t}, \tag{14}$$

$$\frac{\partial Q^{(i)}_{j,k}}{\partial z}\simeq\frac{Q^{(i)}_{j,k+\theta}-Q^{(i)}_{j-1,k+\theta}}{\Delta z}, \tag{15}$$

$$\frac{\partial A^{(i)}_{j,k}}{\partial h}\simeq\left(\frac{\partial A^{(i)}}{\partial h}\right)_{j,k+\theta}. \tag{16}$$

A similar approach is used for the terms $\partial Q(z,t)/\partial t$, $A(z,t)$, $\partial h(z,t)/\partial z$ and $S_f(z,t)$ in Eq. (2). The advection term $\partial(Q^2(z,t)/A(z,t))/\partial z$ is approximated with an upwinding approach:

$$\frac{\partial}{\partial z}\left(\frac{Q^{(i)^2}}{A^{(i)}}\right)_{j,k}\simeq\begin{cases}\dfrac{1}{\Delta z}\left(\left(\dfrac{Q^{(i)^2}}{A^{(i)}}\right)_{j+1,k+\theta}-\left(\dfrac{Q^{(i)^2}}{A^{(i)}}\right)_{j,k+\theta}\right) & Q^{(i)}_{j,k}<0,\\ \dfrac{1}{\Delta z}\left(\left(\dfrac{Q^{(i)^2}}{A^{(i)}}\right)_{j,k+\theta}-\left(\dfrac{Q^{(i)^2}}{A^{(i)}}\right)_{j-1,k+\theta}\right) & Q^{(i)}_{j,k}\geq 0.\end{cases} \tag{17}$$

In this way the two PDEs describing the dynamics of a single channel i are transformed into a system of nonlinear equations:

$$\boldsymbol{f}(\boldsymbol{h}^{(i)}(t_{k+1}),\boldsymbol{h}^{(i)}(t_k),\boldsymbol{q}^{(i)}(t_{k+1}),\boldsymbol{q}^{(i)}(t_k))=\boldsymbol{0}, \tag{18}$$

with $\boldsymbol{h}^{(i)}(t_k)=(h^{(i)}_1(t_k),\ldots,h^{(i)}_N(t_k)^T$, $\boldsymbol{q}^{(i)}(t_k)=(Q^{(i)}_1(t_k),\ldots,Q^{(i)}_{N+1}(t_k)^T$ and $\boldsymbol{f}:\mathbb{R}^{4N^{(i)}+2}\to\mathbb{R}^{2N^{(i)}+1}$. For all the channels Eq. (18) together with all the boundary conditions needs to be solved for $\boldsymbol{h}^{(i)}(t_{k+1})$ and $\boldsymbol{q}^{(i)}(t_{k+1})$ given the values of these variables at time t_k. This can be done with Newton's method. A discussion about the choice of Δt and θ can be found in Clemmens, Bautista, Wahlin, and Strand (2005). A typical value for θ is 0.6 and this is the value used in this paper.

The spatial discretisation parameter Δz is determined by the locations for which the VMM has the actual cross sectional profiles. The value of the spatial discretisation parameter is not equidistant and ranges from 20 m to 70 m. On average it is about 50 m.

4. Three-position controller

A standard three-position controller is used in practice for set-point control and its control actions are based on some very simple rules:

- if the water level is between an upper and lower limit on the set-point, the gate remains unchanged,
- if the water level exceeds the upper limit, then the gate is lowered with a fixed step to lower the water level,
- and if the water level is below the lower limit, then the gate position is increased to increase the water level.

These standard rules are used by the advanced three-position controller installed by the VMM (Flemish Environment Agency) for set-point control during normal operation. During periods of heavy rainfall the working mode of the controllers shifts toward flood control. These standard rules are replaced by new if-then-else rules and were formulated by the local water administration. Based on their many years of experience in controlling the Demer these rules can be considered as expert knowledge. An advantage of this controller is that the gate movement is limited which restricts the wear of the gates. Another advantage is that this type of controller is easily implementable in practice and requires only a very limited number of measurements at every time step. However, the performance of this controller is limited because rain predictions are not taken into account. Furthermore the control actions are only based on local information which has as a consequence that the control actions are not globally optimal.

5. Model Predictive Control

MPC is an optimisation based control strategy which does not suffer from the drawbacks of the three-position controller. At every time step the controller solves an optimisation problem where a process model is used to predict the future outputs within a specified prediction horizon. The effect of rain predictions on future water levels and discharges can be incorporated within the process model. Since the process model is an approximation of the entire river system, the controller will find an optimal solution for the gate positions for the entire river system. MPC is suitable for flood control because safety levels and flood levels can be incorporated as constraints and it can be used at the same time for set-point control because set-points can be used inside the objective function. Only the first element of the entire optimal sequence of control actions is applied to the process, the new current state of the system is measured or estimated and the entire procedure is repeated.

5.1. Choice of control variables and approximate model

The model of the river system derived in Section 3 is too complex to be directly used inside the optimisation problem. To keep the optimisation problem as simple as possible, it is advisable to work with a linear state space model. Because the gate dynamics are too complex to be accurately approximated with a linear model, these gate equations will first be pulled out of the mathematical model of the Demer before deriving the linear model (Breckpot, Agudelo, & De Moor, 2012, 2013). This means that the optimisation problem will work with the gate discharges $Q^{(A)}$, $Q^{(K7)}$ and $Q^{(D)}$ as optimisation variables instead of the gate positions $c^{(A)}$, $c^{(K7)}$ and $c^{(D)}$. After finding the optimal gate discharges, an extra conversion step is needed to find the corresponding gate positions before they can be applied to the process.

The resulting model has the following form:

$$\boldsymbol{x}(k+1)-\boldsymbol{x}_{\text{lin}}=\boldsymbol{A}(\boldsymbol{x}(k)-\boldsymbol{x}_{\text{lin}})+\boldsymbol{B}(\boldsymbol{u}(k)-\boldsymbol{u}_{\text{lin}})+\boldsymbol{D}(\boldsymbol{d}(k)-\boldsymbol{d}_{\text{lin}}) \tag{19}$$

with $\boldsymbol{x}(k)=(\boldsymbol{h}^{(1)^T}(t_k),\ldots,\boldsymbol{h}^{(5)^T}(t_k),h_s(t_k),\boldsymbol{q}^{(1)^T}(t_k),\ldots,\boldsymbol{q}^{(5)^T}(t_k))^T$, $\boldsymbol{u}(k)=(Q^{(A)}(t_k),Q^{(K7)}(t_k),Q^{(D)}(t_k))^T$, $\boldsymbol{d}(k)=(Q_{\text{Dem}}(t_k),Q_{\text{Man}}(t_k))^T$, $\boldsymbol{A}\in\mathbb{R}^{n_x\times n_x}$, $\boldsymbol{B}\in\mathbb{R}^{n_x\times n_u}$ and $\boldsymbol{D}\in\mathbb{R}^{n_x\times n_d}$ with n_x the number of states, n_u the number of inputs and n_d the number of disturbances. The state space matrices are derived for the linearisation points $\boldsymbol{x}_{\text{lin}}$, $\boldsymbol{u}_{\text{lin}}$ and $\boldsymbol{d}_{\text{lin}}$ which correspond to the desired steady state values for the water levels and discharges, the steady state gate discharges and the nominal incoming discharges. Eq. (19) can be rewritten as

$$\boldsymbol{x}(k+1)=\boldsymbol{A}\boldsymbol{x}(k)+\boldsymbol{B}\boldsymbol{u}(k)+\boldsymbol{D}\boldsymbol{d}(k)+\boldsymbol{\beta} \tag{20}$$

with

$$\boldsymbol{\beta}=\boldsymbol{x}_{\text{lin}}-\boldsymbol{A}\boldsymbol{x}_{\text{lin}}-\boldsymbol{B}\boldsymbol{u}_{\text{lin}}-\boldsymbol{D}\boldsymbol{d}_{\text{lin}}. \tag{21}$$

The irregular cross sectional data will not be used in the linearisation procedure. The resulting linear model would only be a good approximation of the nonlinear dynamics locally around the linearisation point. To have a linear model that provides a good approximation for a wide range of water levels and discharges, every irregular profile is first approximated with a trapezoidal profile. The parameters B, S_1 and S_2 of every trapezoidal cross section can be

found by solving the following constrained least squares problem:

$$\min_{B,S} \|\tilde{\boldsymbol{a}} - (\tilde{\boldsymbol{h}}B + \tilde{\boldsymbol{h}}^2 S)\|^2 \tag{22}$$

$$\text{s.t.} B \geq 0,\ S \geq 0 \tag{23}$$

with $\tilde{\boldsymbol{a}} \in \mathbb{R}^m$ a vector of m cross sectional areas corresponding with the m water levels $\tilde{\boldsymbol{h}} \in \mathbb{R}^m$ and $S_1 = S_2 = S$. If one is interested in finding different values for the side slopes, a possible approach is to include the wetted perimeter inside the optimisation problem. However this will turn the least squares problem into a nonlinear optimisation problem. It has been noticed by the authors that solving this more complex optimisation problem has only a minor influence on the resulting value of the parameters and it suffers from local minima. On the right of Fig. 7, the fitting result for an irregular cross section of Dem_3, which is visualised on the left of Fig. 7, can be observed. It is clear that the area of the irregular profile can be approximated accurately with a trapezoidal shape. Another approach could be to fit a trapezoidal shape on the irregular profile itself. However this shape fitting is much more complex to solve and leads to similar results.

As mentioned in Section 3.1, every irregular cross section can have different Manning coefficients for every linear segment. The Manning coefficient for the trapezoidal approximation is taken equal to the equivalent Manning coefficient of the irregular cross section for a given steady state water level.

5.2. The optimisation problem

The optimisation problem that the controller has to solve at every time step is the following Quadratic Programming problem (QP):

$$\min_{\substack{\boldsymbol{u},\boldsymbol{x} \\ \boldsymbol{\xi},\boldsymbol{\zeta}}} \left(\sum_{k=1}^{N_P} \|\boldsymbol{x}(k) - \boldsymbol{r}_x\|_{\boldsymbol{W}}^2 + \sum_{k=0}^{N_P-1} \|\boldsymbol{u}(k) - \boldsymbol{u}(k-1)\|_{\boldsymbol{R}}^2 + \right.$$
$$\left. + \sum_{k=0}^{N_P-1} \|\boldsymbol{u}(k) - \boldsymbol{r}_u\|_{\boldsymbol{U}}^2 + \|\boldsymbol{\xi}\|_{\boldsymbol{S}}^2 + \boldsymbol{s}^T\boldsymbol{\xi} + \|\boldsymbol{\zeta}\|_{\boldsymbol{V}}^2 + \boldsymbol{v}^T\boldsymbol{\zeta} \right) \tag{24}$$

$$\text{s.t. } \boldsymbol{x}(0) = \hat{\boldsymbol{x}}, \tag{25}$$

$$\boldsymbol{x}(k+1) = \boldsymbol{A}\boldsymbol{x}(k) + \boldsymbol{B}\boldsymbol{u}(k) + \boldsymbol{D}\boldsymbol{d}(k) + \tilde{\boldsymbol{\beta}}(k), \quad k = 0, \ldots, N_P - 1 \tag{26}$$

$$\underline{\boldsymbol{u}}(k) \leq \boldsymbol{u}(k) \leq \overline{\boldsymbol{u}}(k), \quad k = 0, \ldots, N_P - 1 \tag{27}$$

$$\boldsymbol{M}^{(i)}\boldsymbol{h}^{(i)}(k) \leq \boldsymbol{M}^{(i)}\boldsymbol{h}^{(i)}_{\max,1} + \mathbf{1}_{n^{(i)}_{\text{con}}} \cdot \eta(k)\xi_i, \quad k = 1, \ldots, N_P, \ i = 1, \ldots, 5 \tag{28}$$

$$\boldsymbol{M}^{(i)}\boldsymbol{h}^{(i)}(k) \leq \boldsymbol{M}^{(i)}\boldsymbol{h}^{(i)}_{\max,2} + \mathbf{1}_{n^{(i)}_{\text{con}}} \cdot \eta(k)\zeta_i, \quad k = 1, \ldots, N_P, \ i = 1, \ldots, 5 \tag{29}$$

$$h_s(k) \leq h^{\text{schulen}}_{\max,1} + \eta(k)\xi_6, \quad k = 1, \ldots, N_P \tag{30}$$

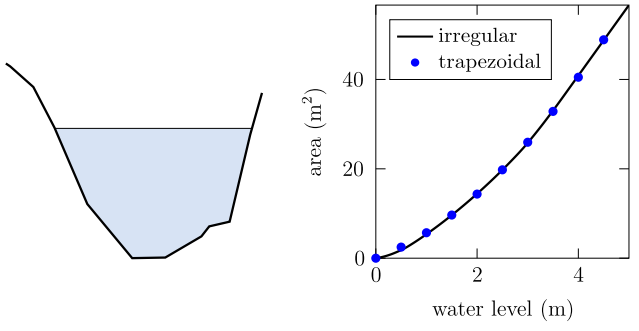

Fig. 7. An irregular cross sectional profile (left) together with its cross sectional area as a function of the water level and its optimal approximation in the least squares sense via a trapezoidal shape.

$$h_s(k) \leq h^{\text{schulen}}_{\max,2} + \eta(k)\zeta_6, \quad k = 1, \ldots, N_P \tag{31}$$

$$\boldsymbol{\xi} \geq 0, \tag{32}$$

$$\boldsymbol{\zeta} \geq 0, \tag{33}$$

with N_P the prediction horizon, $\boldsymbol{W} \in \mathbb{R}^{n_x \times n_x} \geq 0$, $\boldsymbol{R} \in \mathbb{R}^{n_u \times n_u} > 0$, $\boldsymbol{U} \in \mathbb{R}^{n_u \times n_u} \geq 0$, $\boldsymbol{S} \in \mathbb{R}^{6\times 6} > 0$ and $\boldsymbol{V} \in \mathbb{R}^{6\times 6} > 0$ five diagonal weighting matrices, $\boldsymbol{s} \in \mathbb{R}^6$ and $\boldsymbol{v} \in \mathbb{R}^6$ two weighting vectors, $\boldsymbol{r}_x$ the set-points for the states, $\boldsymbol{r}_u$ the set-points for the inputs, $\hat{\boldsymbol{x}}$ the current state estimate of the process, $\tilde{\boldsymbol{\beta}}(k) \in \mathbb{R}^{n_x}$ (defined later on by Eq. (37)), $\boldsymbol{h}_{\max,1}$ the safety levels, $\boldsymbol{h}_{\max,2}$ the flood levels, $\boldsymbol{M}^{(i)} \in \mathbb{R}^{n^{(i)}_{\text{con}} \times N^{(i)}}$ a matrix selecting $n^{(i)}_{\text{con}}$ safety levels and flood levels for the ith reach, $\underline{\boldsymbol{u}}$ and $\overline{\boldsymbol{u}}$ the operational limits on the inputs, $\boldsymbol{\xi} \in \mathbb{R}^6$, $\boldsymbol{\zeta} \in \mathbb{R}^6$ two vectors of slack variables (one slack variable for each reach or reservoir) and $\eta(k) = 1/r_c^{k-1}$ a time-dependent weight (with $r_c > 1$). It can be shown that this QP has only one (global) solution (Nocedal & Wright, 2000). This QP is solved with *cplexqp* of IBM (IBM, 1998). The different aspects of the optimisation problem will now be discussed in the next sections.

5.2.1. The use of slack variables

During periods of heavy rainfall, the safety limits and flood limits can become too restrictive and make the QP infeasible. This is avoided by implementing the flood limits and safety limits as soft constraints (Eqs. (28) and (29)) by using the slack variables $\boldsymbol{\xi}$ and $\boldsymbol{\zeta}$. To keep the violations of these limits as small as possible, the slack variables are penalised in the objective function by the terms $\|\boldsymbol{\xi}\|_{\boldsymbol{S}}^2 + \boldsymbol{s}^T\boldsymbol{\xi}$ and $\|\boldsymbol{\zeta}\|_{\boldsymbol{V}}^2 + \boldsymbol{v}^T\boldsymbol{\zeta}$. A sufficiently large $\boldsymbol{s}$ and $\boldsymbol{v}$ will ensure that the constraints will only be violated when no feasible solution exists for the hard constrained optimisation problem (Hovd & Braatz, 2001). This means that the upper limits on the water levels are enforced as exact soft constraints. If the constraints cannot be prevented from being violated, the controller will minimise these violations and hence reduce the flood risk. The quadratic terms $\|\boldsymbol{\xi}\|_{\boldsymbol{S}}^2$ and $\|\boldsymbol{\zeta}\|_{\boldsymbol{V}}^2$ are included to have a well-posed QP and are extra tuning parameters (Scokaert & Rawlings, 1999). A time-dependent weight $\eta(k)$ is used to penalise future constraint violations in the prediction horizon increasingly to avoid long-lasting constraint violations (Hovd & Braatz, 2001).

Remark. It should be noted that the use of the time-dependent weight $\eta(k)$ can have a negative impact on the control performance. If it is not possible to prevent the river from flooding at the end of the prediction horizon, then the value of the corresponding entry of $\boldsymbol{\zeta}$ will be very large due to the small value of $\eta(N_P)$. This large value for the slack variable can give the controller the freedom to allow large flooding at the beginning of the prediction horizon. This phenomenon did never occur for any of the tests performed in this work. However, if this would occur, the solution is to work with a time-varying vector of slack variables at the cost of an increase in the number of optimisation variables.

5.2.2. Translating the control objectives to the weighting matrices and vectors

The weighting matrices $\boldsymbol{W}$, $\boldsymbol{R}$, $\boldsymbol{U}$, $\boldsymbol{S}$ and $\boldsymbol{V}$ define the relative importance of the difference between the states and their set-points, the changes of the control actions, the difference between the inputs and their set-points and the two vectors of slack variables $\boldsymbol{\xi}$ and $\boldsymbol{\zeta}$ respectively. The buffer capacity of the reservoir above its safety limit cannot be used for keeping the water levels of the channels below their safety limits. Therefore the diagonal element of $\boldsymbol{S}$ and the element of $\boldsymbol{s}$ corresponding to the reservoir will be set higher than the elements associated to the channels. To allow the controller to use the buffer capacity above the safety limit of the reservoir, hence to avoid the river from being flooded, the diagonal elements of $\boldsymbol{V}$ and the elements of $\boldsymbol{v}$ are set higher

than all the elements of $\boldsymbol{S}$ and $\boldsymbol{s}$. If there is no flood risk, the controller needs to focus on set-point control. In this situation the controller should avoid using the reservoir. This is achieved by setting the set-point for the reservoir in $\boldsymbol{r}_x$ equal to 20.4 m TAW in combination with a large weight in the matrix $\boldsymbol{W}$ (but sufficiently smaller than the weights of the slack variables). At the same time $\boldsymbol{r}_u$ for the discharges controlled by gates A and D are set equal to zero together with a large weight on the corresponding diagonal elements of $\boldsymbol{U}$. To keep the downstream water level h_{up} of Dem_1 close to its set-point, the corresponding element in $\boldsymbol{r}_x$ is set equal to 21.5 m TAW in combination with a high element in $\boldsymbol{W}$. All the other elements in $\boldsymbol{r}_x$ are set equal to their steady state values but in combination with a small weighting value. This allows the controller to let these water levels and discharges deviate from their set-points to react on (future) disturbances and keep the effects on h_{up} as small as possible. For the same reason the reference for gate K7 is set equal to its steady state value in combination with a small weighting element in $\boldsymbol{U}$. $\boldsymbol{R}$ influences the control effort of the different input variables. The higher the values in $\boldsymbol{R}$ the smaller the changes in the control actions will be. This means that the controller will react slower and less aggressive than a controller with smaller elements in $\boldsymbol{R}$. However a less aggressive controller will typically lead to less wear on the gates. A trade-off between the reaction speed of the controller and the lifetime of the equipment has to be made.

5.2.3. Nonlinear prediction step

Because the QP works with the gate discharges as optimisation variables, the upper and lower limit of the gates and the rate of change constraint needs to be converted to an upper and lower limit on the gate discharges. Given the current gate position for e.g. gate A at time step $k-1$, the upper and lower limit on the gate discharge for time step k can easily be calculated with

$$\overline{u}^{(A)}(k) = \tilde{f}(c^{(A)}(t_{k-1}) - \Delta^{(A)}_{\max}, h_{\mathrm{up}}(t_k), h_s(t_k)), \tag{34}$$

$$\underline{u}^{(A)}(k) = \tilde{f}(c^{(A)}(t_{k-1}) + \Delta^{(A)}_{\max}, h_{\mathrm{up}}(t_k), h_s(t_k)) \tag{35}$$

with $\Delta^{(A)}_{\max}$ the maximal rate of change for gate A. The same equations hold for gates K7 and D. For calculating the upper and lower limit for the time step $k+1$, an estimation is needed for the states at this time step. In Breckpot et al. (2013), the linear approximate model was used to perform this prediction. However simulations have shown that the prediction with the linear model are not accurate enough when one is working with highly irregular river data for both the bed slopes and the cross sectional profiles. Therefore in this work a nonlinear prediction step is performed with the model of the Demer defined in Section 3. To keep the computation time limited, this prediction step performs only one Newton iteration and the internal time step Δt of the simulator is taken equal to the sampling time of the controller. Before performing this prediction step, the gate positions corresponding with the optimal gate discharges for time step k found by the optimizer in the previous iteration need to be calculated. Since there is a one to one relationship between the gate position and the gate discharge for a given upstream and downstream water level, the corresponding gate position can be easily found by means of a bisection search method. These gate positions are then used in combination with the current state of the system to estimate the water levels and discharges at $k+1$ (denoted with $\boldsymbol{x}_{\mathrm{nonlin}}(k+1)$). Based on $\boldsymbol{x}_{\mathrm{nonlin}}(k+1)$ and $c^{(A)}(k)$, $c^{(D)}(k)$ and $c^{(K7)}(k)$, Eqs. (34) and (35) can now be used to determine $\overline{\boldsymbol{u}}(k+1)$ and $\underline{\boldsymbol{u}}(k+1)$. The same procedure can be used to estimate the time varying upper and lower limits of the gate discharges for the entire prediction window.

The result of this nonlinear prediction step is that the gate discharges are decoupled from the water levels next to the hydraulic structures. However in reality the possible attainable gate discharges does depend on the water levels and these water levels depend on their turn on the gate discharges. Therefore it is possible that the optimizer returns a sequence of gate discharges for which some of these discharges cannot be reached. This can be prevented by iterating over this prediction step and solving the optimisation problem. However the results in Section 7 show that already a good result can be achieved by performing this iteration only once.

5.2.4. Linear model updating

Simulation results show that the accuracy of the linear state space model is good enough for the controller to handle disturbance signals 3.5 times larger than their nominal value. However during periods of heavy rainfall, these disturbance signals can become 8 times larger and the accuracy of the linear state space model is not good enough. This problem can be overcome by performing an update of the linear state space model along the prediction horizon based on the nonlinear predictions. At every time step along the prediction horizon, the estimate of the next state based on the nonlinear model $\boldsymbol{x}_{\mathrm{nonlin}}(k+1)$ is compared with the next state $\boldsymbol{x}_{\mathrm{lin}}(k+1)$ calculated with the linear model:

$$\boldsymbol{x}_{\mathrm{lin}}(k+1) = \boldsymbol{A}\boldsymbol{x}_{\mathrm{nonlin}}(k) + \boldsymbol{B}\boldsymbol{u}(k) + \boldsymbol{D}\boldsymbol{d}(k) + \boldsymbol{\beta}. \tag{36}$$

The simplest way to match the prediction of the linear model with the prediction of the nonlinear model, is to replace $\boldsymbol{\beta}$ with

$$\tilde{\boldsymbol{\beta}}(k) = \boldsymbol{\beta} + (\boldsymbol{x}_{\mathrm{nonlin}}(k+1) - \boldsymbol{x}_{\mathrm{lin}}(k+1)) \tag{37}$$

which will be used inside the optimisation problem (Eq. (26)). Recall that $\boldsymbol{\beta}$ corresponds with the local information contained in the linearisation point (Eq. (21)). By performing this update on $\boldsymbol{\beta}$, this local information is corrected to match the nonlinear state estimates along the prediction horizon.

Another approach would be to use nonlinear MPC and work with time varying state space matrices $\boldsymbol{A}(k)$, $\boldsymbol{B}(k)$ and $\boldsymbol{D}(k)$ derived from linearising the nonlinear model along the nonlinear predicted state estimates. However deriving these linear models at every iteration along the prediction horizon takes a considerable amount of time. This also means that the matrix implementing the equality constraints has to be reconstructed for every iteration. Furthermore the results shown in Section 7 indicate that MPC in combination with the proposed model updating yields already a high performance.

5.2.5. Buffer capacity recovery

After a period of heavy rainfall the controller should recover the buffer capacity as fast as possible to be able to deal with possible future rainfall. This recovery is achieved by changing some of the values in the weighing matrices $\boldsymbol{W}$ and $\boldsymbol{U}$ and the reference signals $\boldsymbol{r}_x$. Once a part of the buffer capacity of the reservoir is used, the water levels of Dem_3 and Dem_4 get a set-point lower than the set-point of the reservoir and their weights in the matrix $\boldsymbol{W}$ are increased. At the same time the weight for h_{up} is decreased. Also the weights of $\boldsymbol{U}$ corresponding with the discharges over gates A and D are decreased. This means that the controller would not keep these discharges close to zero and the controller would have the freedom to use the buffer capacity if there is still a risk of flooding, or to get rid of the excess of water in the reservoir via these gates. This change in $\boldsymbol{W}$, $\boldsymbol{U}$ and $\boldsymbol{r}_x$ is performed when the water level in the reservoir is 20 cm above its set-point. When the water level of the reservoir is at the most 20 cm above its set-point for eight consecutive hours, $\boldsymbol{W}$, $\boldsymbol{U}$ and $\boldsymbol{r}_x$ are set back to their original values.

5.2.6. Controllability of the gates

As mentioned in Section 3.2, the actual gate position has no influence on the gate discharge if the gated weir is in throat control mode. When a gate is in this mode, it can arise that even changing the gate position over a distance $\Delta_{\max}$ results in no change in the gate discharge. This means that the upper limit and lower limit calculated with resp. Eqs. (34) and (35) will have the same value and the controller is not allowed to change the discharge over the gate at that time step. This can happen along the entire prediction window and the controller will stop using this gate: the controller loses one control freedom. This problem can be overcome by keeping the gate in gate control mode or at least on the borderline between both modes. Every time a conversion is made from a gate discharge to a gate position, the bisection search method will return the maximal possible gate position corresponding with the gate discharge. This ensures that Eqs. (34) and (35) will result in different values.

5.2.7. Constraint selection

Not all the flood and safety levels are included inside the optimisation problem as an upper constraint on the water levels. A matrix $\boldsymbol{M}^{(i)} \in \mathbb{R}^{n_{\text{con}}^{(i)} \times N^{(i)}}$ is used to select $n_{\text{con}}^{(i)}$ safety and flood levels for the ith reach. As it will be shown in Section 7, the safety and flood levels are very irregular along every reach. Therefore only the safety and flood levels which are the most critical ones are used inside the optimisation problem. This has the advantage that the complexity of the QP is reduced and the computation time for solving the QP is decreased. The smaller the distance between the flood level and the water level in steady state at a grid point, the more critical this flood level is. The authors conducted a sensitivity analysis on the number of safety and flood levels; it was concluded that this sensitivity is small.

6. State estimator

The current state of the river system needs to be known before the optimisation problem defined in the previous section can be solved. Because only the water levels h_s, h_{up} and h_{down} are measured in practice and none of the discharges, a state estimator is needed. Getting an accurate estimate of the states, especially the water levels, is of a high importance in this application. An estimation error of 5 cm on the water levels can make the difference between flooding and no flooding. Therefore the estimator used in this study will be a combination of a nonlinear prediction step together with a correction step of the classical Kalman filter (Kalman, 1960).

The estimation of the state vector $\boldsymbol{x}(k)$ will be written as $\hat{\boldsymbol{x}}(k)$. The Kalman filter corrects the state estimation based on the linear state space model with the error between the estimated and measured water levels via a feedback gain matrix $\boldsymbol{L}$:

$$\Delta\hat{\boldsymbol{x}}(k+1) = \boldsymbol{L}(\Delta\boldsymbol{y}(k) - \Delta\hat{\boldsymbol{y}}(k)) + \boldsymbol{A}\Delta\hat{\boldsymbol{x}}(k) + \boldsymbol{B}\Delta\boldsymbol{u}(k) + \boldsymbol{D}\Delta\boldsymbol{d}(k), \tag{38}$$

$$\Delta\hat{\boldsymbol{y}}(k) = \boldsymbol{C}\Delta\hat{\boldsymbol{x}}(k) \tag{39}$$

with $\Delta\boldsymbol{x}(k) = \boldsymbol{x}(k) - \boldsymbol{x}_{\text{lin}}$, $\Delta\hat{\boldsymbol{x}}(k) = \hat{\boldsymbol{x}}(k) - \boldsymbol{x}_{\text{lin}}$, $\Delta\boldsymbol{u}(k) = \boldsymbol{u}(k) - \boldsymbol{u}_{\text{lin}}$, $\Delta\boldsymbol{y}(k) = \boldsymbol{y}(k) - \boldsymbol{y}_{\text{lin}}$, $\Delta\hat{\boldsymbol{y}}(k) = \hat{\boldsymbol{y}}(k) - \boldsymbol{y}_{\text{lin}}$, $\boldsymbol{y}(k)$ the measured water levels, $\hat{\boldsymbol{y}}(k)$ the estimated water levels and $\boldsymbol{C}$ a matrix which selects the measured water levels from the states. The Kalman gain $\boldsymbol{L}$ is found by minimising the covariance of the estimation error $\boldsymbol{x}(k) - \hat{\boldsymbol{x}}(k)$ taking process and measurement noise into account. Both types of noise are assumed to be independent and white noise based on a normal distribution. The exact derivation for finding $\boldsymbol{L}$ can be found in Franklin, Powell, and Workman (1997) and Kwakernaak and Sivan (1972).

The accuracy of this state estimator is good enough for disturbance signals 3.5 times larger than their nominal value. However during periods of heavy rainfall, the accuracy of the Kalman filter decreases. This problem can be overcome by replacing the linear prediction step in Eq. (38) with a state estimate based on the nonlinear model $\boldsymbol{x}_{\text{nonlin}}(k+1)$:

$$\hat{\boldsymbol{x}}(k+1) = \boldsymbol{L}(\Delta\boldsymbol{y}(k) - \Delta\hat{\boldsymbol{y}}(k)) + \boldsymbol{x}_{\text{nonlin}}(k+1). \tag{40}$$

$\boldsymbol{x}_{\text{nonlin}}(k+1)$ is found in a similar way as the approach mentioned in Section 5.2.4.

7. Simulation results

In this section the control performance of the proposed MPC are compared with the performance of the currently used three-position controller. The sampling time of both controllers is equal to 15 min, the length of the prediction window N_P is taken equal to 24 h. The disturbance signals are based on the historical rainfall data of the flood event of 2002 and are visualised in Fig. 8. It is assumed that there is no uncertainty on these disturbance signals. Table 1 presents the limits on the three gates. The only variables that are measured at every time step are h_{up}, h_s and h_{down}. For the MPC the other state variables are estimated with the proposed Kalman filter. Unlike the MPC, the three-position controller only requires the measured three water levels for determining the control actions. For Dem_1, Dem_3, Dem_4 and Man_5 only the ten most critical flood levels and safety levels are selected, while for Dem_2 all the six flood and safety levels are taken into account. The control actions of both controllers will be applied to the full hydrodynamic model of the Demer using the irregular bed profiles, the piecewise-linear cross sectional profiles and the Manning roughness coefficients corresponding with every linear segment of these profiles.

Table 2 contains the diagonal elements for the weight matrices $\boldsymbol{W}$, $\boldsymbol{R}$, $\boldsymbol{U}$, $\boldsymbol{S}$ and $\boldsymbol{V}$, and the elements of the weight vectors $\boldsymbol{s}$ and $\boldsymbol{v}$. The chosen values are in line with the reasoning given in Sections 5.2.2 and 5.2.5. During normal operation the controller focuses on keeping the most downstream water level of Dem_1 close to its set-point without using the buffer capacity of the reservoir. This is achieved with the matrices $\boldsymbol{W}$ and $\boldsymbol{U}$. When there is a risk of violating the safety or flood levels, the controller will

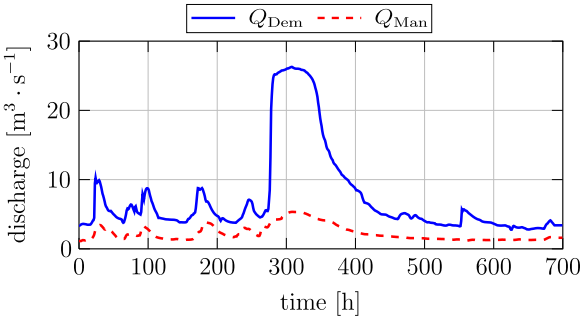

Fig. 8. The inflowing discharges of the Demer and the Mangelbeek based on the historical rainfall data of 2002.

Table 1
Upper and lower limits and maximum rate of change for the gates A, K7 and D.

Gate constraints	Gate A	Gate K7	Gate D
Lower limit (m TAW)	20	20.03	18.9
Upper limit (m TAW)	22.5	23	22.9
$\Delta_{\max}$ (m) each 15 min	0.1	0.1	0.1

Table 2
Diagonal elements for the weight matrices $\boldsymbol{W}$, $\boldsymbol{S}$, $\boldsymbol{V}$, $\boldsymbol{R}$ and $\boldsymbol{U}$, and the elements for the weight vectors $\boldsymbol{s}$ and $\boldsymbol{v}$.

Weight element	Dem_1	Dem_2	Dem_3	Dem_4	Man_5	Schulensmeer
$\boldsymbol{W} \in \mathbb{R}^{534\times534}$						
water levels	$\binom{10^{-3}\cdot\mathbf{1}_{94}}{10}$	$10^{-3}\cdot\mathbf{1}_6$	$10^{-3}\cdot\mathbf{1}_{66}$	$10^{-3}\cdot\mathbf{1}_{11}$	$10^{-3}\cdot\mathbf{1}_{86}$	50
	$\binom{10^{-3}\cdot\mathbf{1}_{94}}{0.01}$[a]		$0.01\cdot\mathbf{1}_{66}$[a]	$0.01\cdot\mathbf{1}_{11}$[a]		
discharges	$10^{-3}\cdot\mathbf{1}_{96}$	$10^{-3}\cdot\mathbf{1}_7$	$10^{-3}\cdot\mathbf{1}_{67}$	$10^{-3}\cdot\mathbf{1}_{12}$	$10^{-3}\cdot\mathbf{1}_{87}$	
$\boldsymbol{S} \in \mathbb{R}^{6\times6}$						
safety levels	10^3	10^3	10^3	10^3	10^3	10^4
$\boldsymbol{s} \in \mathbb{R}^{6\times1}$						
safety levels	10^3	10^3	10^3	10^3	10^3	10^4
$\boldsymbol{V} \in \mathbb{R}^{6\times6}$						
flood levels	10^5	10^5	10^5	10^5	10^5	10^5
$\boldsymbol{v} \in \mathbb{R}^{6\times1}$						
flood levels	10^5	10^5	10^5	10^5	10^5	10^5

	$Q^{(A)}$	$Q^{(K7)}$	$Q^{(D)}$
$\boldsymbol{R} \in \mathbb{R}^{3\times3}$			
control actions	0.01	0.01	0.01
$\boldsymbol{U} \in \mathbb{R}^{3\times3}$			
control actions	1000	0.001	1000
	0.001[a]		0.001[a]

[a] Values used to recover the buffer capacity of the reservoir.

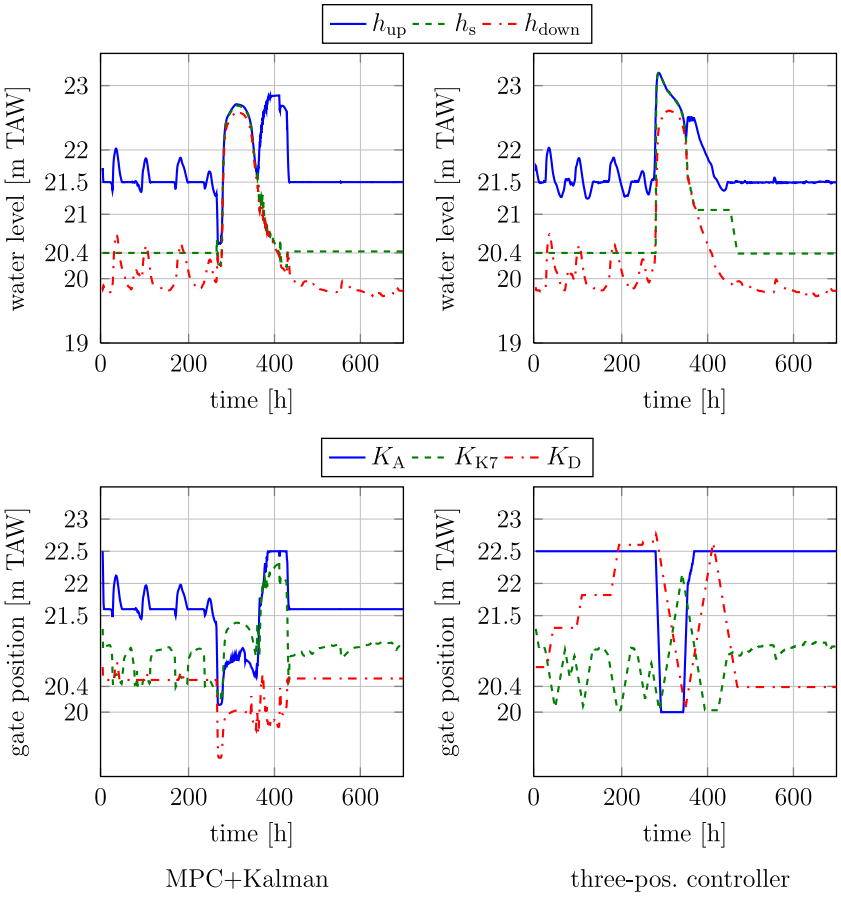

Fig. 9. The evolution of the water levels h_{up}, h_s and h_{down} (top) and the gate positions $c^{(A)}$, $c^{(K7)}$ and $c^{(D)}$ (bottom) for MPC in combination with the Kalman filter (left) and the three-position controller (right). The set-points for h_{up} and h_s are 21.5 m and 20.4 respectively.

automatically try to minimise these violations because of the high values in $\boldsymbol{S}$, $\boldsymbol{s}$, $\boldsymbol{V}$ and $\boldsymbol{v}$. The fast recovery of the buffer capacity after a period of heavy rainfall is achieved by replacing the elements in the matrices $\boldsymbol{W}$ and $\boldsymbol{U}$ with the values marked with a star as indicated in Table 2. The low values in $\boldsymbol{R}$ ensure that the controller has sufficient freedom to achieve its objectives. r_c is taken equal to 1.2 (which was found by trial-and-error).

Fig. 9 shows the results for MPC in combination with the Kalman filter (on the left) and the results for the three-position controller (on the right denoted with three pos. controller). The

top figures show the evolution of the three measured water levels while the bottom figures show the applied control actions for the three gates. MPC succeeds in keeping h_{up} closer to its set-point of 21.5 m TAW by using gate $K7$ than the three-position controller. One reason is because MPC can react on future disturbances. Another reason is that MPC keeps gate $K7$ always inside or at the boundary of its controllable region which has the advantage that MPC can change the discharge over gate $K7$ at any time step, which is not the case with the three-position controller. This controller keeps e.g. decreasing the gate position of this gate when the water level is increasing but without any effect on the resulting gate discharge. Overall MPC attenuates the effect of the bumps in the disturbance signals on h_{up} much better than the three-position controller. Some of these bumps are completely absorbed with MPC. At the beginning of the simulation MPC brings gates A and D, which are initially uncontrollable, immediately at the boundary of their controllable region, without letting water enter the reservoir. These gates remain more or less 10 cm above h_{up}, resp. max(h_s, h_{down}). The three-position controller however keeps gate A constant during the first part of the simulation while it increases the position of gate D without any effect.

Before the period of heavy rainfall starts, MPC lowers the position of the three gates in order to decrease the water levels upstream of the Demer as much as possible. During the period of heavy rainfall it uses the three gates to minimise the floodings along the five reaches. The three-position controller lowers gates A and D to start using the buffer capacity. However because the positions of these gates are too high at the beginning of the heavy rainfall period, the controller reacts too late which results in much higher water levels. Fig. 10 shows the maximal water level for both controllers for each reach together with their flood levels. The area between the flood levels and water levels has a gray colour when flooding takes place with MPC and the area is hatched when flooding takes place with the three-position controller. The maximal water levels obtained after using MPC are always lower than the maximal water levels after the use of the three-position controller. Both controllers prevent Dem_2 and Dem_4 from flooding. MPC prevents Dem_1 from flooding at almost every grid point while the three-position controller results in more and larger floods along this reach. Dem_3 shows flooding for both controllers at only one point, while for Man_5 the flood level overtoppings with MPC are much smaller and at less locations than with the three-position controller. Table 3 shows the maximal flooding, the total flooding (i.e. the sum of the difference between the water level and the flood level, if positive, at each grid point for every reach at every minute) and the flood duration for both controllers for every reach. A negative value for the maximal flooding corresponds with the minimal margin before a flood level is violated. MPC clearly outperforms the three-position controller. The water levels for reaches Dem_2 and Dem_4 and the reservoir are decreased as well as the maximal violation of the flood levels for the other reaches. Also the total flooding and the flood duration improves when MPC is used to control the hydraulic structures.

After the period of heavy rainfall both controllers start emptying the reservoir, hence recovering the buffer capacity of this reservoir. In order to recover this buffer capacity as fast as possible,

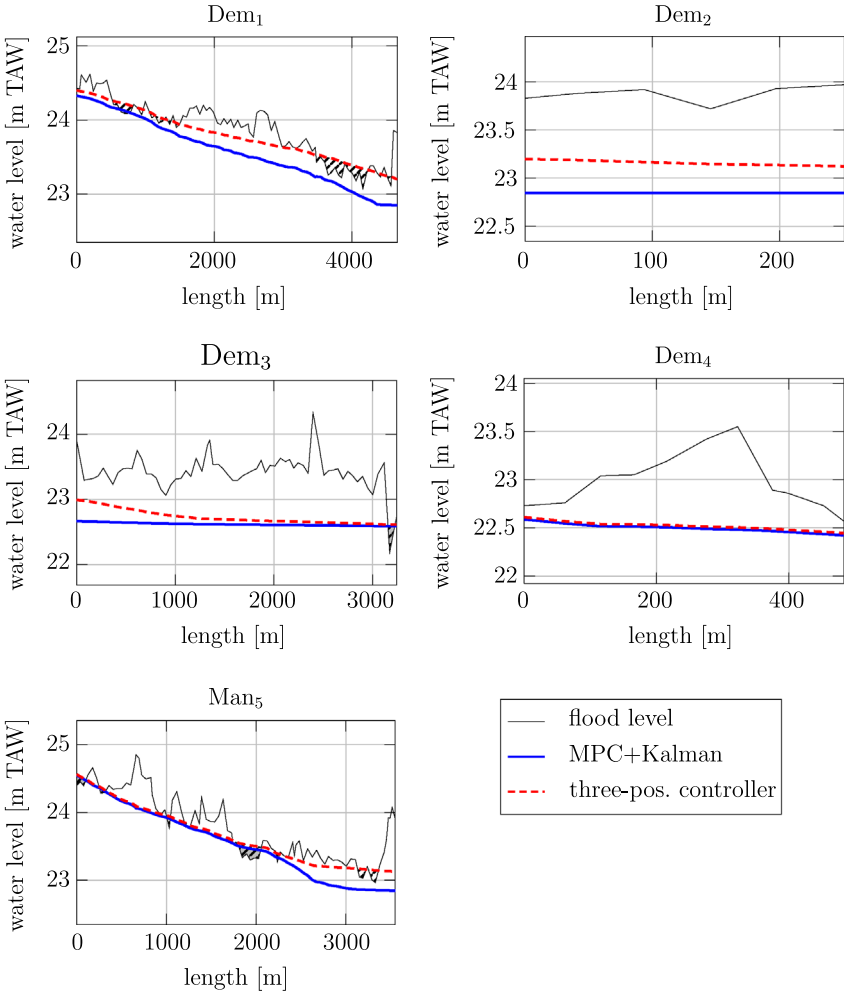

Fig. 10. The maximal water levels for the five reaches for both controllers together with their flood levels.

Table 3
Maximal flooding, total flooding and flood duration for the five reaches and the reservoir for both controllers. The maximal flooding is defined as the maximal difference between the flood level and the water level and the total flooding as the sum of the water level – flood level difference (if positive) at every grid point every minute. A negative value for the maximal flooding corresponds with the minimal margin before a flood level is violated.

Flooding results	Dem_1	Dem_2	Dem_3	Dem_4	Man_5	Schulensmeer
Maximal flooding (m)						
Three-pos. controller	0.275	−0.573	0.432	−0.119	0.216	−0.006
MPC+Kalman	0.036	−0.875	0.409	−0.142	0.168	−0.509
Total flooding (m)						
Three-pos. controller	2877	0	1243	0	4096	0
MPC+Kalman	69	0	1138	0	2032	0
Flood duration (h)						
Three-pos. controller	49.1	0	63.1	0	60.5	0
MPC+Kalman	27.3	0	62.9	0	46.6	0

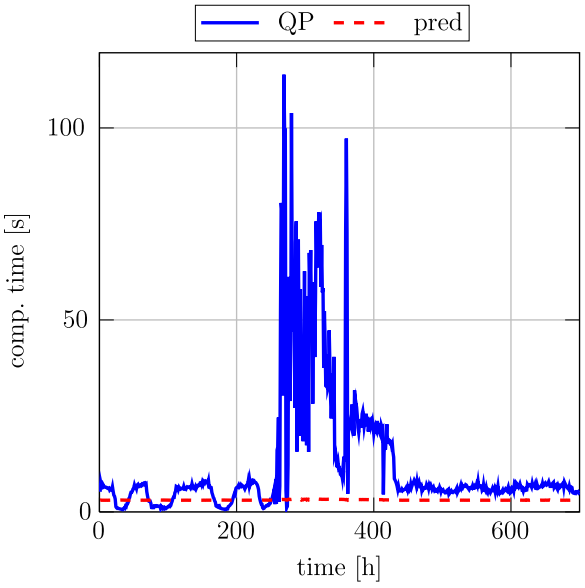

Fig. 11. Computation time needed by the MPC controller to solve the optimisation problem and the nonlinear prediction step at every sampling time (performed on a PC with a 3.1 GHz Intel Core i5 CPU and a RAM of 4 GB using a fast solver).

Table 4
Total gate movement (m) for the three gates for both controllers.

Controller	$c^{(A)}$	$c^{(K7)}$	$c^{(D)}$
Three-pos. controller	5	14.75	9.63
MPC+Kalman	17.16	21.46	16.87

MPC allows the water levels upstream of the Demer to approach their safety limit reducing the amount of water flowing to the reservoir and the downstream part of the Demer. Once the buffer capacity is recovered, MPC starts focussing again on set-point control of h_{up} and it steers this water level back to its set-point. Further bumps in the disturbance signals are completely absorbed by the controller: almost no variations can be seen on h_{up}. The three-position controller recovers the buffer capacity much slower. It also allows h_{up} to increase, however this increase is much smaller than with MPC (keep in mind that the three-position controller does not make use of the flood and safety levels). The decrease of the water level of the reservoir is stalled for 80 h before the last part of the buffer capacity is recovered: the controller needs to wait before gate D becomes lower than the water level of the reservoir. Afterwards the controller steers h_{up} back to its set-point of 21.5 m TAW. However some variation in the water level is visible due to variation in the disturbance signals. MPC succeeds in recovering the buffer capacity in 38 h earlier than the three-position controller and it steers h_{up} back to its set-point 13 h earlier than the three-position controller.

Fig. 11 shows the time needed by the controller to perform the prediction step and the time needed to solve the optimisation problem at every sampling time. The time needed to make the conversion step for the gates after solving the optimisation problem and the time needed for the Kalman filter are negligible (less than 0.015 s, respectively 0.46 s). One can see that the time needed to solve the QP during the period of heavy rainfall stays well below the sampling time. However during this simulation test the state of the Demer is somehow "frozen": while the optimisation problem is being solved, the states of the system are not changing in time while in reality they do. The effect on the control performance needs to be checked. The larger the river system, the bigger this effect will be because of the longer computation time needed to solve the QP. The time for performing the prediction step is more or less the same at every iteration because the nonlinear model is solved with a fixed time step and with only one Newton iteration.

Table 4 shows the quantification of the total amount of control actions for the three controllers. For each gate m the total gate movement is calculated with the formula

$$\gamma^{(m)} = \sum_{k=0}^{N_T-1} |u^{(m)}(k+1) - u^{(m)}(k)| \tag{41}$$

where N_T is the total number of time instants during the simulation. The higher these numbers, the more demanding the controller is for the hydraulic structures. One can see that the three-position controller moves the three gates significantly less than MPC. This is the price that MPC has to pay to keep the gates at all times close to their controllable region. One could reduce these values for MPC by increasing the value of the diagonal elements in the weight matrix $\boldsymbol{R}$. However this will only effect the control actions when the gates are in their controllable regions. If the gate is near to its controllable region (e.g. gates A and D before and after the heavy rainfall period) then this gate will not be kept constant. Therefore the gate will follow the evolution of the surrounding water levels independently of the value used in $\boldsymbol{R}$. One approach to solve this "unnecessary" gate movements would be to first look at the predicted future disturbance signals. If no heavy rainfall would be predicted for the future period, then one could keep the gates connecting the river with the reservoir constant. Once a heavy rainfall event is predicted, the controller can also use these gates for flood prevention. This has the advantage that the amount of gate movement will drastically decrease for these gates.

8. Conclusions and Future work

In this work it is shown how a nonlinear mathematical model of a river system consisting of multiple reaches, gates, junctions and a reservoir can be derived. It is shown that a linear

approximation of this nonlinear model is suitable to be used by the MPC control strategy if one works with gate discharges instead of gate positions as optimisation variables. To get an accurate estimate of the upper and lower limit of the gate discharges at every time step of the prediction window, a fast nonlinear prediction scheme is proposed in this work. The MPC is used in combination with a Kalman filter. The prediction step based on the linear model in the classical Kalman filter has been replaced by a nonlinear prediction step to get accurate enough state estimates. The proposed MPC control strategy is tested on a mathematical model of the Demer, which was constructed using real river data in combination with historical rainfall information of the flooding of 2002. The simulation results showed that MPC outperforms the current control scheme: the number and the magnitude of the floodings were significantly reduced with MPC and the used buffer capacity was recovered in a fast way.

In this work it is assumed that the rain predictions are known at every time step. However in reality there is uncertainty on the weather predictions, especially for predictions further ahead in time. In future work the robustness of the proposed controller against uncertainty on these weather predictions will be examined. In future work the proposed control scheme will also be applied to a larger part of the Demer. In future work other approaches will be checked that can be used to select the most relevant upper limits on the water levels.

Acknowledgments

M. Breckpot is a Ph.D. fellow of the Research Foundation – Flanders (FWO) at the KU Leuven, Belgium, O.M. Agudelo is a post-doctoral researcher at the KU Leuven, Belgium, P. Meert is scientific researcher at the KU Leuven, Belgium, P. Willems is professor at the KU Leuven, Belgium and B. De Moor is a full professor at the KU Leuven, Belgium. The hydro- and geometrical data for the river Demer network were provided by the Flemish Environment Agency (VMM). Research supported by: Research Council KUL: GOA/10/09 MaNet, PFV/10/002 (OPTEC), several PhD/postdoc & fellow grants; Flemish Government: IOF: IOF/KP/SCORES4CHEM, FWO: PhD/post-doc grants, projects: G.0320.08 (convex MPC), G.0558.08 (Robust MHE), G.0557.08 (Glycemia2), G.0588.09 (Brain-machine), G.0377.09 (Mechatronics MPC); G.0377.12 (Structured systems) research community (WOG: MLDM), IWT: PhD Grants, projects: Eureka-Flite+, SBO LeCoPro, SBO Climaqs, SBO POM, O&ODsquare, Belgian Federal Science Policy Office: IUAP P7/ (DYSCO, Dynamical systems, control and optimisation, 2012–2017), IBBT, EU: ERNSI, FP7-EMBOCON (ICT-248940), FP7-SADCO (MC ITN-264735), ERC ST HIGHWIND (259 166), ERC AdG A-DATADRIVE-B, COST: Action ICO806: IntelliCIS, Contract Research: AMINAL, Other: ACCM.

References

Barjas Blanco, T. (2010). *The river Demer controlled by MPC*. Ph.D. Thesis, Leuven, Belgium: Faculty of Engineering, KU Leuven (September).

Barjas Blanco, T., Willems, P., Chiang, P. P.-K., Haverbeke, N., Berlamont, J., & De Moor, B. (2010). Flood regulation using nonlinear model predictive control. *Control Engineering Practice*, *18*, 1147–1157.

Barjas Blanco, T., Willems, P., Po-Kuan Chiang, P., Cauwenberghs, K., & De Moor, B. (2009). *Flood regulation by means of Model Predictive Control. Intelligent infrastructures* (pp. 407–436). Springer.

Breckpot, M., Agudelo, O. M., & De Moor, B. (2012). Modelling of a river system with multiple reaches. In *16th IFAC symposium on system identification* (pp. 1454–1459). Brussels, Belgium.

Breckpot, M., Agudelo, O. M., & De Moor, B. (2013). Flood control with model predictive control for river systems with water reservoirs. *Journal of Irrigation and Drainage Engineering*, *139*(7), 532–541.

Breckpot, M., Barjas Blanco, T., & De Moor, B. (2010). Flood control of rivers with nonlinear model predictive control and moving horizon estimation. In *49th IEEE conference on decision and control* (pp. 6107–6112).

Chaudry, M. H. (2008). *Open-channel flow*. Springer.

Chiang, P.-K., & Willems, P. (2010). A conceptual river model to support real-time flood control (Demer river, Belgium). In: A. Dittrich, K. Koll, J. Aberle, & P. Geisenhainer (Eds.), *River flow*, vol. 2 (pp. 1407–1414). Karlsruhe, Germany: Bundesanstalt für Wasserbau.

Chow, V. T. (1959). *Open-channel hydraulics*. New York, NY: McGraw-Hill Book Co., Inc.

Chow, V. T., Maidment, D. R., & Mays, L. W. (1988). *Applied hydrology, McGraw-Hill series in water resources and environmental engineering*. McGraw-Hill.

Clemmens, A. J., Bautista, E., Wahlin, B. T., & Strand, R. J. (2005). Simulation of automatic canal control systems. *Journal of Irrigation and Drainage Engineering*, *131*(4), 324–335.

Cunge, J. A., Holly, F. M., & Verwey, A. Practical aspects of computational river hydraulics, 1980.

Franklin, G. F., Powell, D. J., & Workman, M. L. (1997). *Digital control of dynamic systems* (3rd ed). Prentice Hall.

Horton, R. E. (1933). Separate roughness coefficients for channel bottom and sides. *Engineering News Record*, *111*(22), 652–653.

Hovd, M., & Braatz, R. D. (2001). Handling state and output constraints in MPC using time-dependent weights. In *Proceedings of the American control conference (ACC)*.

IBM. (1998). IBM ILOG CPLEX V12.1 User's manual for CPLEX.

Innovyze. (2011). InfoWorks-RS Help Documentation [Version 12.0], Innovyze, Oxfordshire, UK.

Kalman, R. E. (1960). A new approach to linear filtering and prediction problems. *Transactions ASME, Series D, Journal of Basic Engineering*, *82*, 34–45.

Kwakernaak, H., & Sivan, R. (1972). *Linear optimal control systems*. New York, NY: Wiley-Interscience.

Litrico, X., & Fromion, V. (2009). *Modeling and control of hydrosystems*. Springer-Verlag.

Mayne, Q., Rawlings, J. B., Rao, C. V., & Scokaert, P. O. M. (2000). Constrained model predictive control: *Stability and optimality*. *Automatica*, *36*(6), 789–814.

Nocedal, J., & Wright, S. J. (2000). *Numerical optimization*. New York, USA: Springer.

Puig, V., Romera, J., Quevedo, J., Cardona, C. M., Salterain, A., Ayesa, E., et al. (2009). Optimal predictive control of water transport systems: *Arrêt-Darré/Arros case study*. *Water Science & Technology*, *60*(8), 2125–2133.

Qin, S., & Badgwell, T. (2003). A survey of industrial model predictive control technology. *Control Engineering Practice*, *11*(7), 733–764.

Rossiter, J. (2003). *Model-based predictive control*. CRC Press.

Scokaert, P. O. M., & Rawlings, J. B. (1999). Feasibility issues in linear model predictive control. *AIChE Journal*, *45*, 1649–1659.

Strelkoff, T. S., & Falvey, H. T. (1993). Numerical methods used to model unsteady canal flow. *Journal of Irrigation and Drainage Engineering*, *119*(4), 637–655.

Sturm, T. W. (2001). *Open channel hydraulics*. McGraw-Hill.

van Overloop, P. J. (2006). *Model predictive control of open water systems*. Ph.D. Thesis, Technische Universiteit Delft, The Netherlands.

van Overloop, P. J., Clemmens, A. J., Strand, R. J., Wagemaker, R. M. J., & Bautista, E. (2010). Real-time implementation of model predictive control on Maricopa–Stanfield irrigation and drainage district's WM Canal. *Journal of Irrigation and Drainage Engineering*, *136*(11), 747–756.

Wahlin, B., & Clemmens, A. J. (2006). Automatic downstream water-level feedback control of branching canal networks: *Theory*. *Journal of Irrigation and Drainage Engineering*, *132*(3), 208–219.

Willems, P., Barjas Blanco, T., Chiang, P.-K., Cauwenberghs, K., Berlamont, J., & De Moor, B. (2008). Real-time control of urban flooding. In: J. Feyen, K. Shannon, & M. Neville (Eds.), *Water & urban development paradigms: Towards an integration of engineering, design and management approaches* (pp. 265–270). CRC Press, Taylor & Francis Group.